Abstract

# Measurement of total hadronic differential cross sections in the LArIAT experiment

Elena Gramellini

2018

Abstract goes here. Limit 750 words.

# Measurement of total hadronic differential cross sections in the LArIAT experiment

A Dissertation
Presented to the Faculty of the Graduate School
of
Yale University
in Candidacy for the Degree of
Doctor of Philosophy

by
Elena Gramellini

Dissertation Director: Bonnie T. Fleming

Date you'll receive your degree

# Contents

# Acknowledgements

A lot of people are awesome, especially you, since you probably agreed to read this when it was a draft.

# Chapter 0

# Liquid Argon Detectors at the Intensity Frontier

In the next few years, LArTPCs will be the tools to answer some of the burning questions in neutrino physics today. This section illustrates the operational principles of this detector technology, as well as the scope of the key detectors in the US liquid argon program – SBN, DUNE and LArIAT.

## 0.1 The Liquid Argon Time Projection Chamber Technology

### 0.1.1 TPCs, Neutrinos & Argon

David Nygren designed the first Time Projection Chamber (TPC) in the late 1970s [23] for the PEP-4 experiment, a detector apt to study electron-positron collisions at the PEP storage ring at the SLAC National Accelerator Laboratory. From the original design in the seventies – a cylindrical chamber filled with methane gas – the TPC detector concept has seen many incarnations, the employment of several different active media and a variety of different particle physics applications, including, but

1

not limited to the study of electron/positron storage rings (e.g. PEP4, TOPAZ, ALEPH and DELPHI), heavy ions collisions in fixed target and collider experiments (e.g. EOS/HISS and ALICE ), dark matter (ArDM), rare decays and capture (e.g. TRIUMP, MuCap), neutrino detectors and nucleon decay (ICARUS, SBN, DUNE), and neutrino less double beta decay (Next). A nice review of the history of TPCs and working principles is provided in [15].

Several features of the TPC technology make these detectors a more versatile tool compared to other ionization detectors and explain such a wide popularity. TPCs are the only electronically read detector which deliver simultaneous three-dimensional track information and a measurement of the particle energy loss. Leveraging on both tracking and calorimetry, particle identification (PID) capabilities are enhanced over a wide momentum range.

Historically, the active medium in ionization detectors has been in the gaseous form. Carlo Rubbia first proposed the use of a Liquid Argon TPC for a neutrino experiment, ICARUS [27], in 1977. Using nobles elements in the liquid form for neutrino detectors is advantageous for several reasons. The density of liquids is ∼1000 times greater than gases, increasing the number of target centers for neutrino's interaction in the same volume. Since the energy loss of charged particle is proportional to the target material density, as shown in the Bethe-Block equation, eq. 1, the increased density reflects into a proportionally higher energy loss, enhancing the calorimetry capability of detectors with a liquid active medium. Additionally, the ionization energy of liquids is smaller than gasses by the order of tens of eV. Thus, at the passage of charged particles, liquid generally produce more ionization electrons than gas for the same deposited energy and force the particles to deposit more energy in a shorter range. The downside of using noble liquid gasses in experiments is that they require expensive cryogenic systems to cool the gas until it transitions to its the liquid form. The properties of liquid argon in comparison liquid xenon – a popular choice for dark

| Element | LAr | LXe |
|---|---|---|
| Atomic Number | 18 | 54 |
| Atomic weight A | 40 | 131 |
| Boiling Point Tb at 1 atm | 87.3 K | 165.0 K |
| Density | 1.4 g/cm$^3$ | 3.0 g/cm$^3$ |
| Radiation length | 14.0 cm | 2.8 cm |
| Moliere Radius | 10.0 cm | 5.7 cm |
| Work function | 23.6 eV | 15.6 eV |
| Electron Mobility at $E_{field} = 10^4$ V/m | 0.047 m$^2$/Vs | 0.22 m$^2$/Vs |
| Average dE/dx MIP | 2.1 MeV/cm | 3.8 MeV/cm |
| Average Scintillation Light Yield | 40000 $\gamma$/MeV | 42000 $\gamma$/MeV |
| Scintillation $\lambda$ | 128 nm | 175 nm |

Table 1: LAr, LXe summary of properties relevant for neutrino detectors.

matter and neutrinoless double beta decay detectors – are summarized in table 1. Albeit xenon would be more desirable than argon given some superior properties such as lower ionization energy and higher density and light yield, argon relative abundance abates the cost of argon compared to xenon, making argon a more viable choice for the construction of kilo-ton scale neutrino detectors.

LArTPCs are some times referred as to "electronic" bubble-chambers, for the similarity in the tracking and energy resolution which is coupled with an electronic readout of the imaging information in LArTPCs. Compared to these historic detectors however, LArTPC bestow tridimensional tracking and a self triggering mechanism provided by the scintillation light in the noble gas. An event display of a $\nu_\mu$ CC interaction candidate in the MicroBooNE detector is shown in picture 1 to display the level of spatial details these detectors a capable of; the color scale of the image is proportional to the energy deposited, hinting to the calorimetry capabilities of the detectors.

## 0.1.2    LArTPC: Principles of Operation

To the bare bones, a LArTPC is a bulk of liquid argon sandwiched in a flat capacitor, equipped with a light collection system. A uniform electric field of the order of
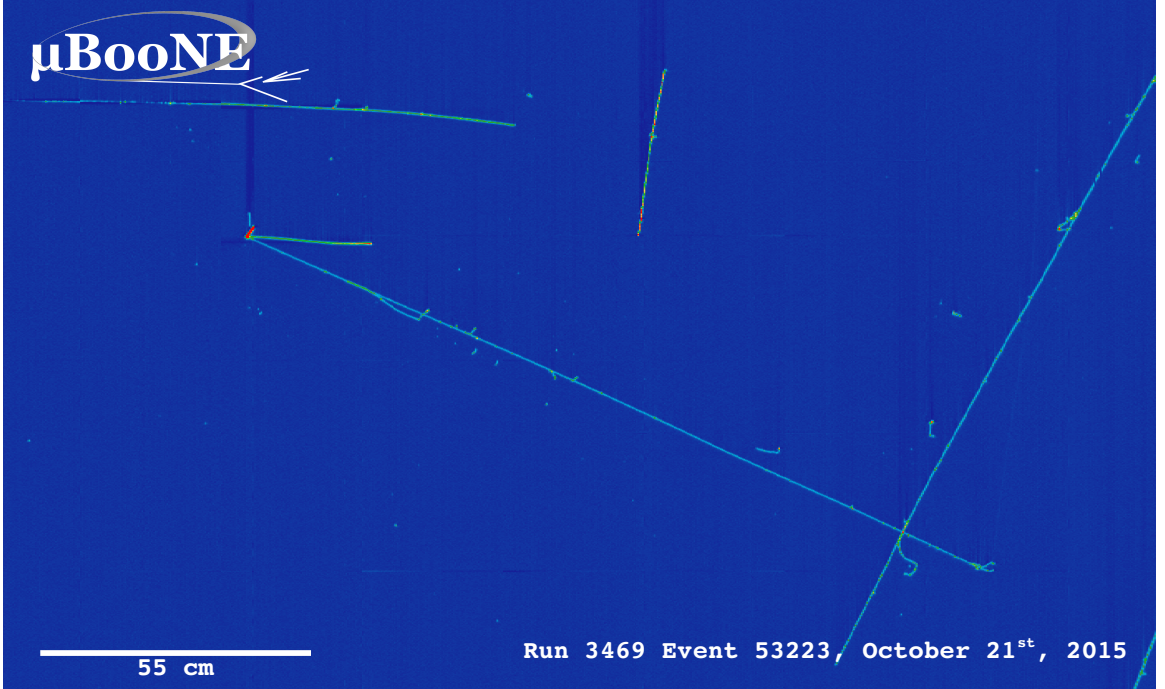
Figure 1: Event display of a $\nu_\mu$ CC interaction candidate in the MicroBooNE detector.

500 V/cm is maintained constant between the faces of the capacitor. The anode is sensitive to ionization charge and it is usually made of two or more planes segmented into several hundreds parallel sense wires a few millimeters apart; different geometries for the anode segmentation are under study [11].

Argon ionization and scintillation are the processes leveraged to detect particles in the LArTPC active volume. When a ionizing radiation traverses the argon active volume it leaves a trail of ionization electrons along its trajectory and it excites the argon producing of scintillation light – details on the production and detection of ionization charge and scintillation light are provided in 0.1.4 and 0.1.4 respectively. The optical the detector sees the argon scintillation light in matters of nanoseconds. This flash of light determines the start time of an event in the chamber, $t_0$. The uniform electric field drifts the ionization electrons from the production point towards the anode in order of hundreds of microseconds or more depending on the chamber dimensions[1]. The anode sense wires see either an induced current by the drifting

1. The ionized argon also drifts, but in the opposite directions compared to the electrons. Since

charge (on induction planes) or an injection of the ionization charge (collection plane). An appropriate choice of the voltage bias on each wire plane assures ideal charge transparency, so that all the ionization charge is collected on the collection plane and none on the induction planes.

The arrival time of the charge on the anode sense wires is used to measure the position of the original ionizing radiation in the drift direction. In fact, since the constant electric field implies that the drift velocity is also constant, the position of the original ionization is simply given by the multiplication of the drift velocity by the drift time, where the "drift time" is the difference between $t_0$ and the charge arrival time on the wire planes. The spacial resolution on this dimension is limited by the time resolution of the electronics or by longitudinal diffusion of the electrons. The spatial information on the different wire planes maps a bi-dimensional projection of the interaction pattern in the plane perpendicular to the drift direction. The spacial resolution on this dimension is limited by the transverse electron diffusion in argon and by the grain of the anode segmentation, i.e. the spacing between the wires in the sense planes [10]. The off-line combination of the 2-D information on the wire planes with the timing information allows for the 3D reconstruction of the event in the chamber.

Since the charge deposited by the ionizing radiation is proportional to the deposited energy and the charge collected on the sense plane is a function of the deposited charge, LArTPC allow the measurement of the energy deposit in the active volume. Effects due to the presence of free charge and impurities in the active volume, such as a finite electron lifetime, recombination and space charge, complicate the relationship between deposited and collected charge affecting the measurement of the particle's energy, as described in the next section.

---

the drift time is proportional to the particle mass, the ions' drift time is much longer than the electrons'. Ionized argon is collected on the cathode which is not instrumented, so it is not used to infer information about the interactions in the chamber.

### 0.1.3 Liquid Argon: Ionization Charge

The mean rate of energy loss by moderately relativistic elementary charge particles heavier than electrons is well described by the modified Bethe-Bloch [25] equation

$$-\frac{dE}{dx} = Kz^2\frac{Z}{A}\varrho\frac{1}{\beta^2}\left[\frac{1}{2}\ln\frac{2m_ec^2\beta^2\gamma^2T_{max}}{I^2} - \beta^2 - \frac{\delta}{2}\right],\qquad(1)$$

where $z$ is the number of unit charge of the ionizing radiation, $Z$, $A$ and $\varrho$ are the atomic number, mass number and density of the medium, $m_e$ is the electron mass, $\gamma = \frac{\beta}{\sqrt{1-\beta^2}}$ is the Lorentz factor of the ionizing radiation, $T_{max}$ is the maximum kinetic energy which can be imparted to a free electron in a single collision, $I$ is the mean excitation energy on eV, $\delta$ is the density correction and $K = 0.307075$ MeV g$^{-1}$ cm$^2$ is a numerical conversion factor. The Bethe-Bloch treats the energy loss by an ionizing radiation via quantum-mechanical collisions producing ionization or an excitation in the medium as an uniform and continuous process. The density correction terms becomes relevant for incident particle with high energy, where screening effects due to the polarization of the medium by high energy particles occur.

Excitation and ionization of the detector medium occur in similar amounts. Since the ionizing collisions occur randomly, we can parametrize their number $k$ in a segment of length $s$ along the track with a Poissonian function

$$P(k) = \frac{s^k}{k!\lambda^k}e^{-s/\lambda},\qquad(2)$$

where $\lambda = 1/N_e\sigma_i$, with $N_e$ being the electron density of $\sigma_i$ the ionization cross-section per electron. About 66% of the ionizing collisions in Argon produce only a single electron/ion pair [15]; in the other cases, the transferred kinetic energy is enough for the primary electron to liberate one or more secondary electrons, which usually stay close to the original pair. Occasionally, electrons can receive enough energy to

be ejected with high energy, forming so-called "$\delta$-ray": a detectable ionization short track off the particle trajectory, as shown in figure 2. The average number of $\delta$-ray with energy E>E$_0$ per cm follows the empirical form

$$P(E > E_0) \sim \frac{y}{\beta^2 E_0},\qquad(3)$$

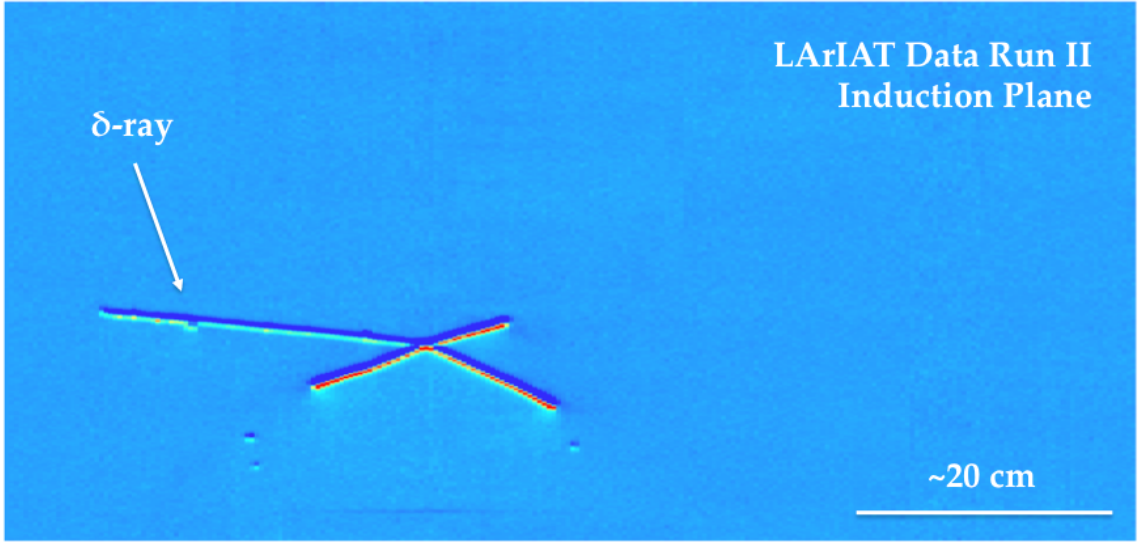where $y$ is an empirical factor depending on the medium (0.114 for gaseous Ar), and $\beta$ is $v/c$.



Figure 2: Events display for a LArIAT pion absorption candidate on the induction plane, with highlighted delta ray.

**Purity & Electron Life Time**

The presence of electronegative contaminants in liquid argon, such as oxygen and water, is particularly pernicious, since these molecules quench the charge produced by the ionizing radiation. Thus, amount of charge per unit of length $dQ/dx$ collected on the collection plane depends on the charge's production point in the detector: ionization produced close to the cathode will see more impurities along its journey to the collection plane than ionization produced close to the anode, resulting in greater

attenuation of its charge. As a result, the amount of charge collected on the sense wires as a function of the traveled distance follows an exponential decay trend. The traveled distance is generally measured in terms of drift time and the characteristic time constant of the exponential decay is called electron lifetime $\tau_e$. Figure 3 shows the typical life time for LArIAT data. The procedure to measure the electron lifetime in LArIAT is outlined in [26]. LArIAT small drift distance (47 cm) allows for a relatively short electron life time. The life time for bigger detectors such as MicroBooNE, whose drift distance is 2.5 m, needs to be of the order of tens of milliseconds to allow charge collection usable for physics analyses. Energy reconstruction in LArTPC applies a correction for the finite lifetime to calibrate the detector calorimetric response; details for LArIAT are provided in Section ??.
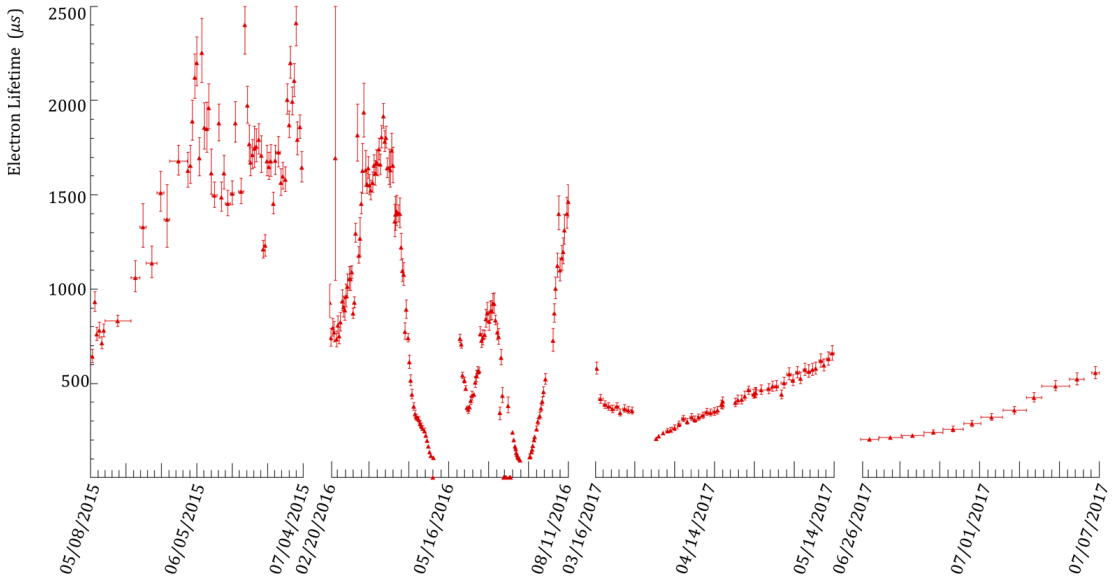


Figure 3: Electron lifetime during the LArIAT run period [9].

LArTPCs use hermetically sealed and leak-checked vessels to abate the leakage and diffusion of contaminants into the system. The liquid argon filling of the volume occurs after the vessel is evacuated or purged with gaseous argon [3] to reduce remaining gases in the volume. Even so, the construction of a pure tank of argon is unviable, as several sources of impurity remain. In particular, impurities can come from the raw argon supply, the argon filtration system and from the outgassing from internal surfaces. Outgassing is a continuous diffusive process producing contaminants, especially water, even after the vessel is sealed, particularly from materials in the ullage region[2]. Since research-grade argon comes from the industrial distillation of air, the impurities with the highest concentration are nitrogen, oxygen and water, generally maintained under the 1 part per million level by the vendor. Even so, a higher level of purity is necessary to achieve a free electron life time usable in meter scale detectors. Thus, argon is constantly filtered in the cryogenic system, which reduce the oxygen and water contamination to less than 100 parts per trillion. The filtration system depends on the size and drift distance of the experiment and, for experiments on several meters scale, it includes an argon recirculation system.

**Recombination Effect**

After production, ionization electrons thermalize with the surrounding medium and may recombine with nearby ions. Recombination might occur either between the electron and the parent ion through Coulomb attraction, as described in the geminate theory [24], or thanks to the collective charge density of electrons and ions from multiple ionizations in a cylindrical volume surrounding the particle trajectory, as described in the columnar model [17]. Consideration on the average electron-ion distance and the average ion-ion distance for argon show that the probability of

---

2. While the liquid argon low temperature reduces outgassing in the liquid, this process remains significant for absorptive material (such as plastic) above the surface of the liquid phase.

geminate recombination is low; thus recombination in argon is mainly due to collective effects [1]. Since protons, kaons and stopping particles present a higher ionization compared to MIPs, recombination effects are more prominent when considering the reconstruction of energy deposited by these particles.

Models for a theoretical descriptions of recombination based on the Birks model and the Box model are provided in [6] and [29], respectively. The Birks model assumes a gaussian spatial distribution around the particle trajectory during the entire recombination phase and identical charge mobility for ions and electrons. The Box model also assumes that electron diffusion and ion mobility are negligible in liquid argon during recombination. In these models, the fraction of ionization electrons surviving recombination is a function of the number of ion-electron pairs per unit length, the electric field, the average ion-electron separation distance after thermalization and the angle of the particle with respect to the direction of the electric field – plus the diffusion coefficient in the Birks model. Given the stringent assumptions, it is perhaps not surprising that these models are in accordance to data only in specific regimes: the Birks model is generally used to describe recombination for low dE/dx, the Box model for high dEdX. In LArTPC, the ICARUS and ArgoNeut have measured recombination in [4] and [1] respectively. Since LArIAT uses the refurbished ArgoNeut TPC and cryostat at the same electric field, LArIAT currently corrects for recombination using the ArgoNeut measured recombination parameters in [1].

**Space Charge Effect**

Slow-moving positive argon ions created during ionization can build-up in LArTPC, causing the distortion of the electric field within the detector. This effect, called "space charge effect" leads to a displacement in the reconstructed position of the signal ionization electrons. In surface LArTPCs the space charge effect is primarily due to the rate of ionization produced by cosmic rays which is slowly drifting in the

chamber at all times. Surface LArTPC of the size of several meters are expected to be modestly impacted from the space charge effect, where charge build-up create anisotropy of the electric field magnitude of the order of 5% at a drift field of 500 V/cm [21]. The smallness of the LArIAT drift volume is such that effect of space charge on the electric field is expected to be even smaller. CHIEDI A FLAVIO

### 0.1.4 Liquid Argon: Scintillation Light

Liquid argon emits scintillation light at the passage of charged particles. LArTPCs leverage this property to determine when the ionization charge begins to drift towards the anode plane.

**Scintillation Process**

Scintillation light in argon peaks in the ultraviolet at a 128 nm, shown in comparison to Xenon and Kypton in Figure 4, from [22]. The light yield collected by the optical detector depends on the argon purity, the electric field, the dE/dx and particle type, averaging at the tens of thousands of photons per MeV.

The de-excitation of Rydberg dimers in the argon is responsible for the scintillation light. Rydberg dimers exist in two states: singlets and a triplets. The time constant for the singlet radiative decay is 6 ns, resulting in a prompt component for the scintillation light. The decay of the triplet is delayed by intersystem crossing, producing a slow component with a time constant of $\sim$ 1500 ns. "Self-trapped exciton luminescence" and "recombination luminescence" are the two processes responsible for the creation of the Rydberg dimers [19]. In the first process, a charged particle excites an argon atom which becomes self-trapped in the surrounding bulk of argon, forming a dimer; the dimer is in the singlet state 65% of the times and in the triplet state 35% of the times. In case of recombination luminescence, the charged particle transfers enough energy to ionize the argon. The argon ion forms a charged argon dimer state,
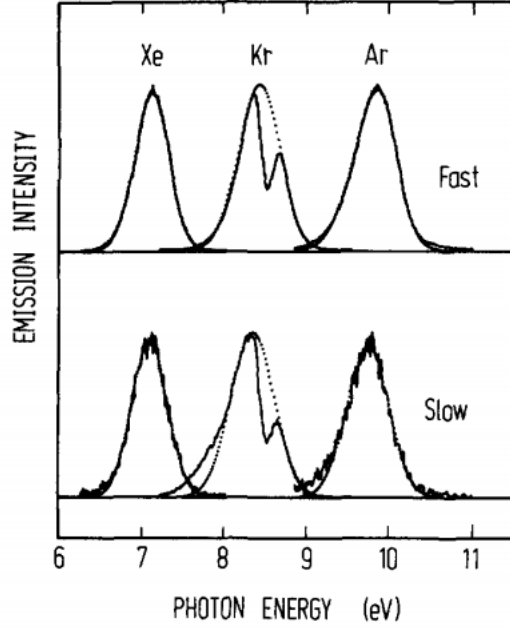
Figure 4: Emission spectra of the fast and slow emission components in Xenon, Kypton and Argon according to [22]. The dotted lines correspond to the Gaussian fits.

which quickly recombines with the thermalized free electron cloud. Excimer states are produced in the recombination, roughly half in the singlet and half in the triplet state. The light yield dependency on the electric field, on the dE/dx and particle type derives from the role of free charge in the recombination luminescence process. The spacial separation between the argon ions and the free electron cloud depends on the electric field. On one hand, a strong electric field diminishes the recombination probability, leading to a smaller light yield; on the other, it increases the free charge drifting towards the anode plane. Hence, the amount of measurable charge and light anti-correlates as a function of the electric field. Ionizing particles in the argon modify the local density of both free electrons and ions depending on their dE/dx. Since the recombination rate is proportional to the square of the local ionization density, highly ionizing particles boost recombination and the subsequent light yield compared to MIPs. The possibility to leverage this dependency for pulseshape-based particle identification has been shown in [7, 20].

12

**Effects Modifying the Light Yield**

The production mechanism through emission from bound excimer states implies that argon is transparent to its own scintillation light. In fact, the photons emitted from these metastable states are not energetic enough to re-excite the argon bulk, greatly suppressing absorption mechanisms. In a LArTPC however, several processes modify the light yield in between the location where light is produced and the optical detector. In a hypothetical pure tank of argon, Rayleigh scattering would be the most important processes modifying the light yield. Rayleigh scattering changes the path of light propagation in argon, prolonging the time between light production and detection. The scattering length has been measured to be 66 cm [16] , shorter than the theoretical prediction of $\sim$ 90 cm [28]; this value is short enough to be relevant for the current size of LArTPCs detectors. In fact, Rayleigh scattering worsen the resolution on $t_0$, the start time for charge drifting, and alters the light directionality, complicating the matching between light and charge coming from the same object in case of multiple charged particles in the detector.

Traces of impurities in argon such as oxygen, water and nitrogen also affect the light yield, mainly via absorption and quenching mechanisms. Absorption occurs as the interaction of a 128 nm photon directly with the impurity dissolved in the liquid argon. Differently, quenching occurs as the interaction of an argon excimer and an impurity, where the excimer transfers its excitation to the impurity and dissociates non-radiatively. Given this mechanism, it is evident how quenching is both a function of the impurity concentrations and the excimer lifetime. Since the triplet states live much longer than the singlet states, quenching occurs mainly on triplet states, affecting primarily the slow component of the light, reducing the scintillation yield and a shortening of the scintillation time constants.

The stringent constraints for the electron life time limit the presence of oxygen and water to such a low level that both absorption and quenching on these impurity is not

expected to be significant. Contrarily, the nitrogen level is not bound by the electron life time constraints – nitrogen being an inert gas, expensive to filter. Thus, nitrogen is often present at the level provided by the vendor. The effects of nitrogen on argon scintillation light have been studied in the WArP R&D program and at several test stands. The quenching process induced by nitrogen in liquid Ar has been measured to be proportional to the nitrogen concentration, with a rate constant of $\sim 0.11$ $\mu s^{-1}$ ppm$^{-1}$; appreciable decreasing in lifetime and relative amplitude of the slow component have been shown for contamination as high as a few ppm of nitrogen [2]. For a nitrogen concentration of 2 parts per million, typical of the current generation of LArTPC, the attenuation length due to nitrogen has been measured to be $\sim$30 meters [18].

**Wavelength Shifting of LAr Scintillation Light**

Liquid argon scintillation light is invisible for most optical detectors deployed in a LArTPC, such as cryogenic PMTs and SiPMs, since a wavelength of 128 nm is generally too short to be absorbed from most in glasses, polymers and semiconductor materials. Research on prototype SiPMs absorbing directly VUV light and their deployment in noble gasses experiment is ongoing but not mature [30]. Thus, experiments need to shift the wavelength of scintillation light to be able to detect it. Albeit deployed in different ways, neutrinos and dark matter experiments commonly use 1,1,4,4-tetraphenyl-butadiene (TPB) to shift the scintillation light. TPB absorbs the vacuum ultraviolet (VUV) light and emits in the visible at $\sim$ 425 nm [8], with a ratio of visible photon emitted per VUV photon absorbed of $\sim$1.2:1 [14].

Neutrino experiments typically coat their optical detector system evaporating a layer of TPB either directly on the PMTs glass surface or on acrylic plates mounted in front of the PMTs [12]; this technique allows the fast detection light coming directly from the neutrino interaction. Dark matter experiments typically evaporate TPB on

reflective foils mounted on the inside walls of the sensitive volume and detect the light after it has been reflected; this technique leads to a higher and more uniform light yield, though scattering effects for both the visible and VUV light augment the propagation time and hinder directionality information [13]. In order to take advantage of both these techniques, hybrid systems with PMT coating and foils are being considered for the next generation of large neutrino detectors.

### 0.1.5   Signal Processing and Event Reconstruction

In this section we illustrate the processing and reconstruction chain of the TPC signals, from the pulses on the sense wire to the construction of three dimensional objects with associated calorimetry.

**Deconvolution.** Induction and collection planes have different field responses, given the different nature of the signals on these planes: the wires on the induction planes see inductive signal of the drifting charge, while the wires on the collection planes see the current derived from the charge entering the conductor. Thus, signals on the induction plane are bi-polar pulse and signal on the collection plane are unipolar pulses, see Figure ADD PULSES FIGURE. The first step in signal processing is deconvolution, that is a series of off-line algorithms geared towards undoing the detector effects. The result of the deconvolution step is the production of a comparable set waveforms on all planes presenting unipolar, approximately gaussian-like pulses. Signal from all planes are treated on equal footage beyond this point. Some LArTPC apply noise filtering in the frequency domain just after the deconvolution to clean up wire cross talk. Since signals from the LArIAT TPC are extremely clean, noise filtering is not necessary.

**Hit Reconstruction.** The second stage of the signal processing is the recon-

struction of hits, indicating an energy deposition in the detector. A peak finder scans the deconvolved TPC waveforms for each wire on the whole readout time looking for spikes above the waveform's baseline. It then fits these peaks with gaussian shapes and stores the fit parameters such as the quality of the fit, the peak time, height and area under the gaussian fit. The information resulting fron this process a single spike form a single reconstructed "hit". The next steps in the event reconstruction chain will then decide if rejecting hits with poor fits. It is important to notice how the height and width of the hit depend on the topology of the event: for example, a particle running parallel to the wire planes will leave a series of sharp hits on many consecutive wires, while a particle traveling towards the planes will leave a long, wide hit on very few wires. The height of the hits and their integral is proportional to the charge collected on the wire, so it depends on the particle type.

The event reconstruction chain uses collection of hits to form more complex objects associated with the particles in the detector. The development of different approaches to accomplish this task is an extremely hot topic in LArTPC event reconstruction which spans from more traditional approaches such as line-clustering [**?**] argoneut paper to the use of machine learning tools [**?**] KAZU'S paper. Generally speaking, the scope of hit clustering and event reconstruction to provide shower-like or track like-objects with an associated energy reconstruction. This is because different particles have different topology in the detector – electrons and photon create electromagnetic showers, resulting in shower-like topologies, while muons and hadrons leave track-like signals. For the scope of these thesis, we will describe only LArIAT's approach to track reconstruction even if we recognize the breath of LArTPC event reconstruction is much wider. We are interested in the reconstruction of pions and kaons in the active volume, whose topology is track-like.

**2D Clustering Reconstruction.** The LArIAT reconstruction of track-like ob-

jects starts by clustering hits on the collection and induction planes separately with the use of the TrajCluster clustering package [**?**] Bruce. TrajCluster looks for a collection of hits in the wire-time 2D space which can be described with a line-like 2D trajectory. TrajCluster reconstructs trajectories by adding trajectory points to the leading edge of the trajectory while stepping through the 2D space of hits. Several factors determine whether a hit is added to the trajectory, including but not limited to

1. the goodness of the fit of the single hit,

2. the charge of the hit compared to the average charge and RMS of the hits already forming the trajectory,

3. the goodness of trajectory fit with and without the hit addition,

4. the angle between the two lines formed by the collection of hits before and after the considered hit in the trajectory.

**3D TrackReconstruction.** The 3D tracking set of algorithms uses clusters close in time on the induction and collection planes as starting point to form a 3D track. Firstly, it construct a tentative 3D trajectory using the edges of the clusters. Then, it projected back the tentative trajectory on to the planes and adjusts the parameters of the 3D track fit such that they minimize the distance between the fit projections and the track hits in all wire planes simultaneously. The track algorithm can use multiple clusters in one plane, but it can never break them in smaller groups of hits. This algorithm was first developed for the ICARUS collaboration [5].

## 0.2    The Intensity Frontier Program

### 0.2.1    SBN: Neutrino Interaction and Detection

### 0.2.2    DUNE: Rare Decay Searches

DUNE will achieve a wide non-accelerator physics program. The key elements for a rare decay experiment are: massive active volume, long exposure, high identification efficiency and low background. Figure 5 shows the current best experimental limits on nucleon decay lifetime over branching ratio (dots). Historically, the dominant technology used in these searches has been water Cherenkov detectors: all the best experimental limits on every decay mode are indeed set by Super-Kamiokande [?, ?]. It is particularly important to notice that the kaon energy for the proton decay mode $p \rightarrow K^+\bar{\nu}$ is under Cherenkov threshold. Super-Kamiokande set the limit on the lifetime for the $p \rightarrow K^+\bar{\nu}$ mode by relying on photons from nuclear de-excitation and on the muon tagging in the kaon decay leptonic mode. For this reason, an attractive alternative approach to identifying nucleon decay is the use of a Liquid Argon Time Projection Chamber (LArTPC).

LArTPCs can complement nucleon decay searches in modes where water Cherenkov detectors are less sensitive, especially $p \rightarrow K^+\bar{\nu}$. According to [?], DUNE will have an active volume large enough, have sufficient shielding from the surface, and will run for lengths of time sufficient to compete with Hyper-K, opening up the opportunity for the discovery of nucleon decay.

### 0.2.3    Enabling the next generation of discoveries: LArIAT

LArIAT, a small Liquid Argon Time Projection Chamber (LArTPC) in a test beam, is designed to perform an extensive physics campaign centered on charged particle cross section measurements while characterizing the detector performance for future
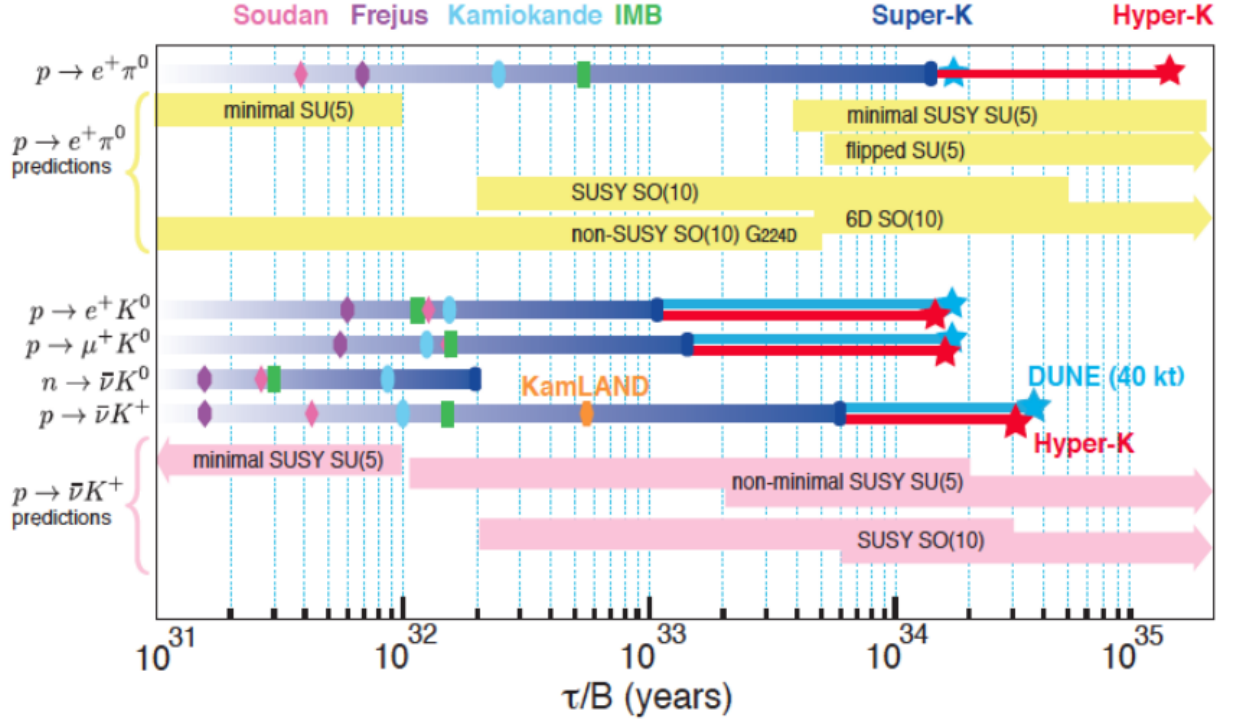
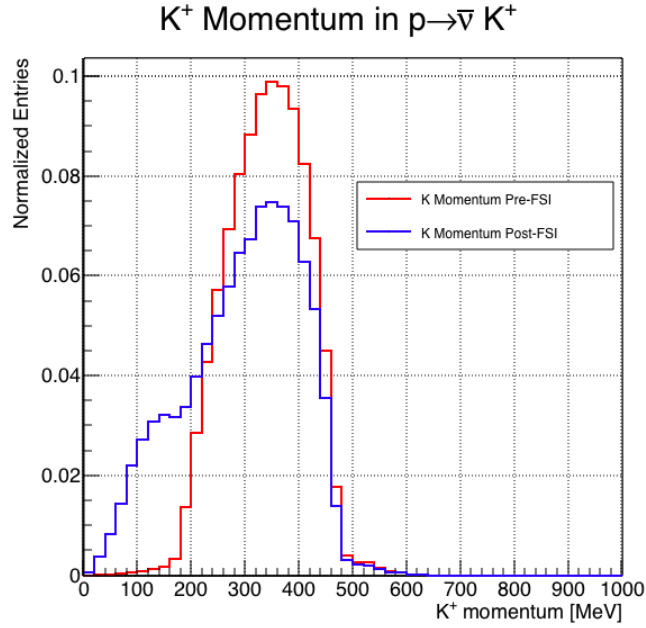Figure 5: Proton decay lifetime limits from passed and future experiments.



Figure 6: Momentum of the kaon outgoing a proton decay event as simulated by the Genie 2.8.10 event generator in argon. The red line represent the kaon momentum distribution before undergoing the simulated final state interaction inside the argon nucleus, while the blue line represents the momentum distribution after FSI.

LArTPCs. LArTPC represents one of the most advanced experimental technologies for physics at the Intensity Frontier due to its full 3D-imaging, excellent particle identification and precise calorimetric energy reconstruction. This complex technology however needs a thorough calibration and dedicated measurements of some key quantities to achieve the precision required for the next generation of discoveries at the Intensity Frontier which LArIAT can provide.

The LArIAT LArTPC is deployed in a dedicated calibration test beamline at Fermilab. We use the LArIAT beamline to characterize the charge particles before they enter the TPC: the particle type and initial momentum is known from beamline information. The precise calorimetric energy reconstruction of the LArTPC technology enables the measurement of the total differential cross section for tagged hadrons. The Pion-Nucleus and Kaon-Nucleus total hadronic interaction cross section have never been measured before in argon and they are a fundamental step to shed light on light meson interaction in nuclei. Additionally, these measures provides a key input to neutrino physics and proton decay studies in future LArTPC experiments like SBN and DUNE. add paragraph on all wonderful things lariat can do... some event displays would be nice!

ADD genie proton decay kaon distribution and lariat beamline overlaied The signature of a proton decay event in the "LAr golden mode" is the presence of a single kaon of about 400 MeV in the detector.

# Bibliography

[1] R Acciarri, C Adams, J Asaadi, B Baller, T Bolton, C Bromberg, F Cavanna, E Church, D Edmunds, A Ereditato, S Farooq, B Fleming, H Greenlee, G Horton-Smith, C James, E Klein, K Lang, P Laurens, D McKee, R Mehdiyev, B Page, O Palamara, K Partyka, G Rameika, B Rebel, M Soderberg, J Spitz, A M Szelc, M Weber, M Wojcik, T Yang, and G P Zeller. A study of electron recombination using highly ionizing particles in the argoneut liquid argon tpc. *Journal of Instrumentation*, 8(08):P08005, 2013.

[2] R Acciarri, M Antonello, B Baibussinov, M Baldo-Ceolin, P Benetti, F Calaprice, E Calligarich, M Cambiaghi, N Canci, F Carbonara, F Cavanna, S Centro, A G Cocco, F Di Pompeo, G Fiorillo, C Galbiati, V Gallo, L Grandi, G Meng, I Modena, C Montanari, O Palamara, L Pandola, G B Piano Mortari, F Pietropaolo, G L Raselli, M Roncadelli, M Rossella, C Rubbia, E Segreto, A M Szelc, S Ventura, and C Vignoli. Effects of nitrogen contamination in liquid argon. *Journal of Instrumentation*, 5(06):P06003, 2010.

[3] M Adamowski, B Carls, E Dvorak, A Hahn, W Jaskierny, C Johnson, H Jostlein, C Kendziora, S Lockwitz, B Pahlka, R Plunkett, S Pordes, B Rebel, R Schmitt, M Stancari, T Tope, E Voirin, and T Yang. The liquid argon purity demonstrator. *Journal of Instrumentation*, 9(07):P07005, 2014.

[4] S. Amoruso et al. Study of electron recombination in liquid argon with the ICARUS TPC. *Nucl. Instrum. Meth.*, A523:275–286, 2004.

[5] M. Antonello, B. Baibussinov, P. Benetti, E. Calligarich, N. Canci, S. Centro, A. Cesana, K. Cieslik, D. B. Cline, A. G. Cocco, A. Dabrowska, D. Dequal, A. Dermenev, R. Dolfini, C. Farnese, A. Fava, A. Ferrari, G. Fiorillo, D. Gibin, S. Gninenko, A. Guglielmi, M. Haranczyk, J. Holeczek, A. Ivashkin, J. Kisiel, I. Kochanek, J. Lagoda, S. Mania, A. Menegolli, G. Meng, C. Montanari, S. Otwinowski, A. Piazzoli, P. Picchi, F. Pietropaolo, P. Plonski, A. Rappoldi, G. L. Raselli, M. Rossella, C. Rubbia, P. Sala, A. Scaramelli, E. Segreto, F. Sergiampietri, D. Stefan, J. Stepaniak, R. Sulej, M. Szarska, M. Terrani, F. Varanini, S. Ventura, C. Vignoli, H. Wang, X. Yang, A. Zalewska, and K. Zaremba. Precise 3d track reconstruction algorithm for the ICARUS t600 liquid argon time projection chamber detector. *Advances in High Energy Physics*, 2013:1–16, 2013.

[6] J B Birks. Scintillations from organic crystals: Specific fluorescence and relative response to different radiations. *Proceedings of the Physical Society. Section A*, 64(10):874, 1951.

[7] Mark G. Boulay and A. Hime. Direct WIMP detection using scintillation time discrimination in liquid argon. 2004.

[8] W. M. Burton and B. A. Powell. Fluorescence of tetraphenyl-butadiene in the vacuum ultraviolet. *Applied Optics*, 12(1):87, jan 1973.

[9] The LArIAT Collaboration. The liquid argon in a testbeam (lariat) experiment. Technical report, In Preparation 2018.

[10] S.E. Derenzo, A.R. Kirschbaum, P.H. Eberhard, R.R. Ross, and F.T. Solmitz. Test of a liquid argon chamber with 20 m rms resolution. *Nuclear Instruments and Methods*, 122:319 – 327, 1974.

[11] A Ereditato, C C Hsu, S Janos, I Kreslo, M Messina, C Rudolf von Rohr, B Rossi, T Strauss, M S Weber, and M Zeller. Design and operation of argontube: a 5 m long drift liquid argon tpc. *Journal of Instrumentation*, 8(07):P07002, 2013.

[12] R. Acciarri et al. Design and construction of the MicroBooNE detector. *Journal of Instrumentation*, 12(02):P02017–P02017, feb 2017.

[13] C. E. Aalseth et al.l. DarkSide-20k: A 20 tonne two-phase LAr TPC for direct dark matter detection at LNGS. *The European Physical Journal Plus*, 133(3), mar 2018.

[14] V.M. Gehman, S.R. Seibert, K. Rielage, A. Hime, Y. Sun, D.-M. Mei, J. Maassen, and D. Moore. Fluorescence efficiency and visible re-emission spectrum of tetraphenyl butadiene films at extreme ultraviolet wavelengths. *Nuclear Instruments and Methods in Physics Research Section A: Accelerators, Spectrometers, Detectors and Associated Equipment*, 654(1):116 – 121, 2011.

[15] H J Hilke. Time projection chambers. *Reports on Progress in Physics*, 73(11):116201, 2010.

[16] N. Ishida, M. Chen, T. Doke, K. Hasuike, A. Hitachi, M. Gaudreau, M. Kase, Y. Kawada, J. Kikuchi, T. Komiyama, K. Kuwahara, K. Masuda, H. Okada, Y.H. Qu, M. Suzuki, and T. Takahashi. Attenuation length measurements of scintillation light in liquid rare gases and their mixtures using an improved reflection suppresser. *Nuclear Instruments and Methods in Physics Research Section A: Accelerators, Spectrometers, Detectors and Associated Equipment*, 384(2-3):380–386, jan 1997.

[17] George Jaffé. Zur theorie der ionisation in kolonnen. *Annalen der Physik*, 347(12):303–344, 1913.

[18] B J P Jones, C S Chiu, J M Conrad, C M Ignarra, T Katori, and M Toups. A measurement of the absorption of liquid argon scintillation light by dissolved nitrogen at the part-per-million level. *Journal of Instrumentation*, 8(07):P07011, 2013.

[19] Benjamin J. P. Jones. *Sterile Neutrinos in Cold Climates*. PhD thesis, MIT, 2015.

[20] W. H. Lippincott, K. J. Coakley, D. Gastler, A. Hime, E. Kearns, D. N. McKinsey, J. A. Nikkel, and L. C. Stonehill. Scintillation time dependence and pulse shape discrimination in liquid argon. *Phys. Rev. C*, 78:035801, Sep 2008.

[21] M. Mooney. The microboone experiment and the impact of space charge effects. 2015.

[22] E. Morikawa, R. Reininger, P. Gürtler, V. Saile, and P. Laporte. Argon, krypton, and xenon excimer luminescence: From the dilute gas to the condensed phase. *The Journal of Chemical Physics*, 91(3):1469–1477, aug 1989.

[23] D. R. Nygren. The time projection chamber: A new $4\pi$ detector for charged particles. Technical report, 1974.

[24] L. Onsager. Initial recombination of ions. *Phys. Rev.*, 54:554–557, Oct 1938.

[25] C. Patrignani et al. Review of Particle Physics. *Chin. Phys.*, C40(10):100001, 2016.

[26] T. Yang R. Acciarri, M. Stancari. Determination of the electron lifetime in lariat. Technical report, March 2016.

[27] C. Rubbia. The Liquid Argon Time Projection Chamber: A New Concept for Neutrino Detectors. 1977.

[28] R. K. Teague and C. J. Pings. Refractive index and the lorentz–lorenz function for gaseous and liquid argon, including a study of the coexistence curve near the critical state. *The Journal of Chemical Physics*, 48(11):4973–4984, jun 1968.

[29] J. Thomas and D. A. Imel. Recombination of electron-ion pairs in liquid argon and liquid xenon. *Phys. Rev. A*, 36:614–616, Jul 1987.

[30] N Yahlali, L M P Fernandes, K Gonzlez, A N C Garcia, and A Soriano. Imaging with sipms in noble-gas detectors. *Journal of Instrumentation*, 8(01):C01003, 2013.